Near–Atomic Resolution Imaging of Ferroelectric Liquid Crystal Molecules on Graphite by STM

David M. Walba,* Forrest Stevens, Daniel C. Parks,
Noel A. Clark, Michael D. Wand

Near–atomic resolution images of a two-dimensional heteroepitaxial crystal composed of the relatively "functionally rich" chiral liquid crystal mesogen MDW 74 on graphite have been obtained by scanning tunneling microscopy (STM). This work is aimed at developing an improved understanding of the commercially crucial phenomenon of liquid crystal alignment by studying well-characterized surfaces. Herein is reported molecular-level characterization of the surface underlying a ferroelectric liquid crystal in situ, a requisite starting point for understanding the liquid crystal–solid interface at the molecular level. The results are also important in the context of developing a model for the molecular origins of the contrast observed in STM images of organic monolayers on conductor surfaces. The data and analysis provide strong evidence that neither frontier orbital alone (highest occupied or lowest unoccupied molecular orbital) is sufficient to describe the observed tunneling efficiency.

It is known from previous work that when a small sample of liquid crystal (LC) is placed on the (0001) surface of highly oriented pyrolytic graphite (HOPG), the adsorbed molecules can sometimes be observed by STM (*1*, *2*). By far the most studied LC class in this regard is the cyanobiphenyls (*3*), and careful analysis of high-resolution STM images of cyanobiphenyls on graphite has provided the following proposals: (i) The images derive from two-dimensional (2D) crystalline monolayers strongly adsorbed on the surface, with bulk liquid crystal overlying these 2D crystals; (ii) the bulk LC phase is not directly observed by STM; (iii) the molecules adsorbed onto the surface perturb the local tunneling efficiency in such a way that the aromatic parts of the molecules appear "bright" in the image (enhanced tunneling efficiency) and the aliphatic parts of the molecules appear "dark" (reduced tunneling efficiency) (*1*); and (iv) the 2D crystals grow on the graphite heteroepitaxially. This previous literature suggests that STM provides an excellent approach for molecular-level characterization of the solid surface (2D heteroepitaxial crystals) underlying an LC film in situ and thus could develop into a powerful tool for understanding LC alignment.

Only a few STM observations of liquid crystals more complex than the cyanobiphenyls have been reported. Most of these have been at molecular resolution (*4*); although in previous work from our laboratories, near–atomic resolution was reported (*5*). For the present study, the enantiomerically pure ferroelectric LC MDW 74 (Fig. 1) (*6*), possessing a chiral epoxide unit, was chosen for the following reasons: First, the neat material shows LC phases close to room temperature. Second, because very little data regarding the behavior of organic functional groups—other than aromatic units and alkyl or alkoxy groups—in STM are available, the presence of functional groups such as the epoxide unit seemed especially interesting.

The STM samples were prepared by placing a small amount (<1 mg) of liquid crystal on a freshly cleaved surface of HOPG. The sample was heated to about 60°C to melt the liquid crystal into the isotropic phase and was then cooled slowly to near room temperature. Scanning tips were prepared from mechanically cut 0.025-cm platinum-iridium (80:20) wire. Typical scanning conditions were 1.0 nA and 0.6 V (tip positive). Most images were obtained in constant current mode at 5.8 Hz (scan lines per second; 400 lines per image). Images were taken in air with a commercial STM (Nanoscope II, Digital Instruments) fitted with a homebuilt heater for operation at slightly above room temperature (T = 38° to 44°C) to prevent crystallization of the LC overlayer.

Images of 2D crystals of MDW 74 were reproducible (similar images were acquired on different days and with different samples of MDW 74) but were not predictable. About two-thirds of the experimental sessions produced no images, or only very poor images. Images showing periodic structure on the 3-nm scale were obtained in 37 sessions.

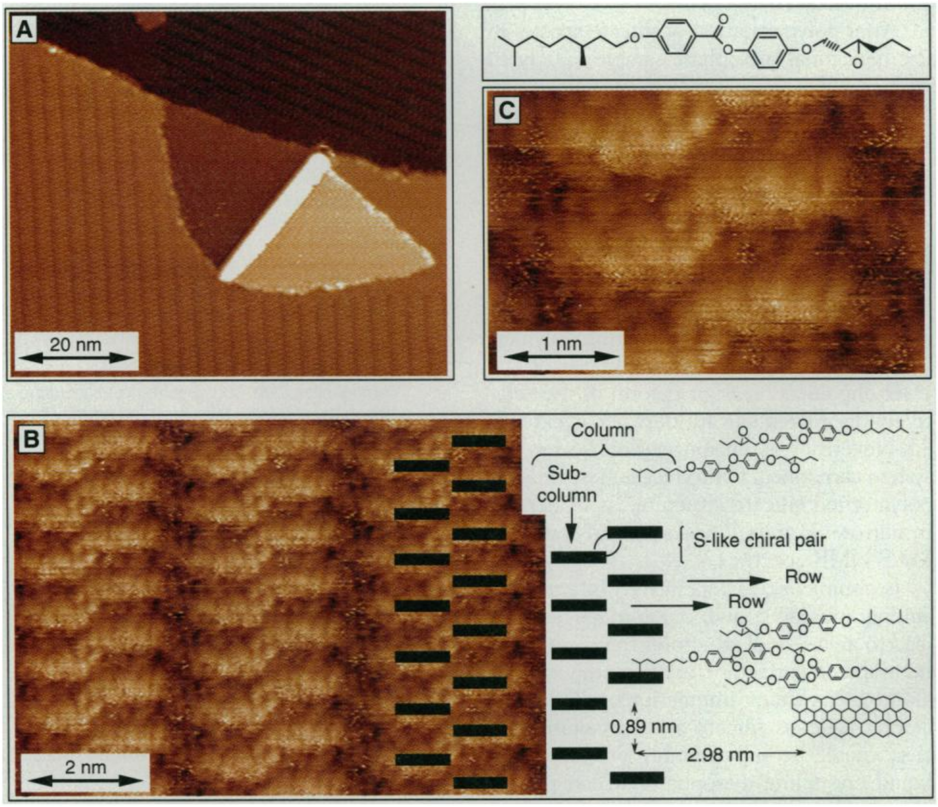

Fig. 1. Three of the best STM images of MDW 74. All images are raw data and were taken under conditions of constant current, 600 mV (tip positive), 1.0 nA, and 5.8 Hz. Image sizes are **(A)** 75 nm by 60 nm, **(B)** 9 nm by 6 nm, and **(C)** 4 nm by 3 nm. These images are cropped from original scan sizes of (A) 100 nm, (B) 10 nm, and (C) 5 nm. In (B), the crystal is also shown in schematic form, with each dark bar representing a phenylbenzoate unit.

D. M. Walba and F. Stevens, Department of Chemistry and Biochemistry and Optoelectronic Computing Systems Center, Campus Box 215, University of Colorado, Boulder, CO 80309–0215, USA.
D. C. Parks and N. A. Clark, Department of Physics and Optoelectronic Computing Systems Center, Campus Box 390, University of Colorado, Boulder, CO 80309–0390, USA.
M. D. Wand, Displaytech, 2200 Central Avenue, Boulder, CO 80301, USA.

*To whom correspondence should be addressed.

Molecular resolution or better was observed in 21 of these sessions, and clean near–atomic resolution was observed in one session (7). Most of the images obtained in these 21 sessions appear consistent with the same crystal structure imaged at different resolutions. The "best" session provided 17 separate images at various scan dimensions that may be considered qualitatively better than all the rest. Three images representative of these 17 are shown in Fig. 1. Figure 1A shows a 75 nm by 60 nm area with a very clear graphite step. A two–graphite layer fold about 25 nm in length is also seen. Two similar 2D crystals with different orientations can be observed in this image, one at each level of the step. Figure 1, B and C, shows the crystal on the higher (brighter) step at 10 nm by 6 nm and 4 nm by 3 nm scales (these images were scanned at a higher resolution than the image in Fig. 1A and are not simply magnifications).

The images are composed of bright columns separated by dark regions. At higher resolution, the bright columns seem to be composed of two ladder-shaped subcolumns of alternating dark and bright regions (Fig. 1B). The "rungs" of the ladders in the subcolumns are all in register, forming well-defined equally spaced rows. There is also considerable structure in the darker regions, especially within the subcolumns, and the images in a monodomain exhibit near (but not precise) twofold symmetry about the z axis (normal to the graphite plane).

Autocorrelation analysis (5) of eight images of MDW 74 from the best session gave a unit cell with axes measuring 0.89 ± 0.05 and 2.98 ± 0.03 nm at an angle of 91° ± 3° (Fig. 1B). The long axis of the unit cell is very close to the molecular length of MDW 74 in an extended conformation (3.0 nm), suggesting that the rows of the structure are composed of molecules arranged end-to-end (either head-to-head or head-to-tail). The length of the bright areas within a subcolumn is 1.4 to 1.6 nm (the "fuzzy" edges of this area make precise measurement difficult), which is slightly longer than the distance between terminal phenolic oxygens of the phenylbenzoate core of MDW 74 (1.2 nm). On the basis of the observed length of the bright regions and given the excellent precedent that aromatic units appear bright in STM while aliphatic groups are dark, it can be assumed that the bright regions in the columns are composed mainly of phenylbenzoate units.

In the set of highest resolution images (such as those shown in Fig. 1), these phenylbenzoate units exhibit a polar structure in the xy plane. More specifically, for each bright region in a subcolumn, "left" is not the same as "right" because of the presence of a very distinctive hooklike feature at the end of each bright unit connecting the bright units of the two subcolumns. The presence of this feature suggests that molecules in adjacent rows within a column are rotated 180° about the z axis and that the arrangement within a row is head-to-tail.

Because adjacent rows appear antiparallel with dark alkyl regions separating bright aromatic regions within the subcolumns, the short axis of the unit cell corresponds to two molecular widths. If the phenylbenzoate units were flat and parallel to the graphite, the spacing between bright regions within a subcolumn could not be less than about 1.1 nm (the width of an aryl ring plus the width of an aliphatic chain). However, a Cambridge Crystal Database search (8) revealed that nearly all phenylbenzoates have a ring-ring dihedral of 70° to 90° in 3D organic crystals, and this conformation can be easily accommodated within the 0.89 nm of space observed between bright regions.

Alkanes in an all-anti conformation are known to adsorb onto graphite in a commensurate fashion such that the plane defined by the carbon chain is parallel to the graphite surface, and the hydrogens on the α face (that is, the side facing the graphite surface) fit into the centers of the graphite rings (geometrically, this fit is very good, imperfect by only about 2%) (9). Good evidence for this type of heteroepitaxial crystal growth of LC mesogens on graphite has been reported from our laboratories on

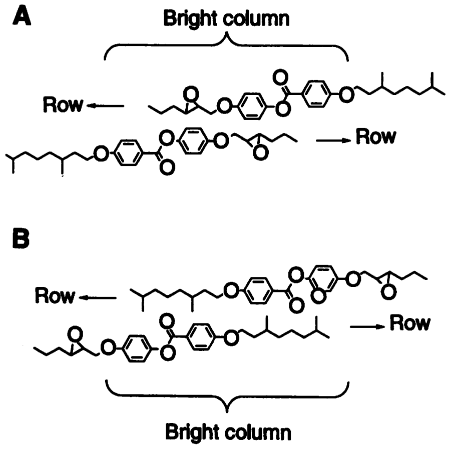

Fig. 2. MDW 74 molecules can be paired in two ways to reproduce the broad features of the STM images. In both cases, the phenylbenzoate units are slightly overlapped, but in (**A**) orientation A, the molecules are paired at the shorter epoxyalkoxy tails, whereas in (**B**) orientation B, the molecules are paired at the longer alkoxy tails. Orientation A was chosen in the modeling work because the "hooks" at the paired ends of the phenylbenzoates are considered to be related to the epoxide units.

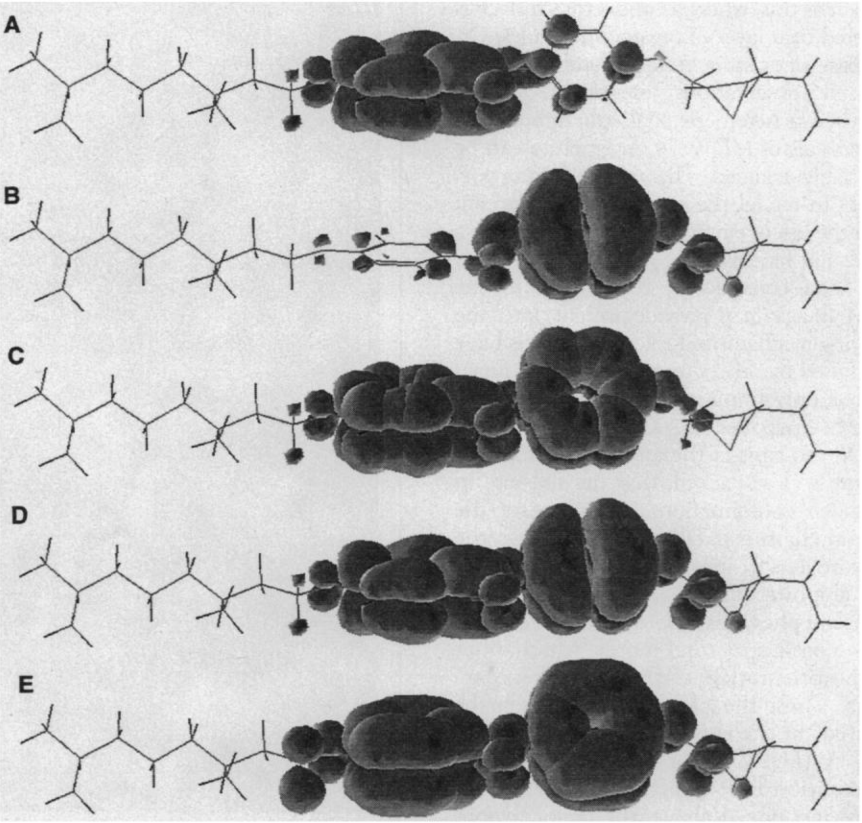

Fig. 3. The frontier molecular orbitals of MDW 74 as calculated by Spartan (Wavefunction) semiempirical MNDO. (**A**) LUMO; (**B**) HOMO; (**C**) superposition of the lowest four unoccupied orbitals; (**D**) superposition of the HOMO and LUMO; and (**E**) superposition of the highest four occupied orbitals.

the basis of observation of coexisting 2D crystalline and stacking-disordered phases at near atomic resolution (*5*).

Furthermore, it has proven possible to obtain images of molecules under a certain set of imaging conditions and then to change the bias voltage to afford an image of the graphite in the same location (*10*). In the few cases where such data have been acquired on MDW 74, the molecular rows are parallel to a graphite lattice vector, consistent with heteroepitaxial growth.

Additional evidence for heteroepitaxial growth in the MDW 74 case is as follows: (i) The 2D crystal domains separated by the four–graphite layer step shown in Fig. 1A are rotated by 60°, consistent with heteroepitaxy; and (ii) the unit cell measured for crystals of MDW 74 (0.89 ± 0.05 nm, 2.98 ± 0.03 nm, 91° ± 3°) is in good agreement with that predicted for an epitaxial crystal as described above (0.852 nm, 2.952 nm, 90.0°). In this model, each row of the crystal is along a graphite lattice vector, the molecule-molecule spacing in a row is 12 graphite vector lengths, and adjacent rows are spaced by [2 × (one graphite vector length) × cos(30°)].

Detailed molecular-level interpretation of the observed STM images is difficult because a theory for the observed contrast in tunneling microscopy is not available in cases such as this, where a conductor's surface is covered by a layer of organic molecules. On the basis of existing literature and the experimental observations mentioned above, however, a heteroepitaxial structure for the 2D crystals of MDW 74 on graphite can be justifiably assumed. This provides an opportunity to model the structure of the crystal with the use of empirical force fields. Once a molecular model of the adsorbed monolayer has been constructed, comparison to the STM image may provide insight into the imaging mechanism. Molecular models have been used by others to interpret STM images, but only minimal molecular mechanics have been applied to such models (*11*).

On the basis of the assumptions that the crystal is close-packed, that the tails are in extended conformations, the plane of the carbon chain is parallel to the surface, the α hydrogens fit into the centers of rings on the graphite surface, and the bright regions are phenylbenzoate units, we consider two basic structural motifs, which differ in the orientation of the phenylbenzoate units. Thus, the phenylbenzoates can be "paired" at the epoxyalkoxy tails [orientation A (Fig. 2A)] or at the alkoxy tails [orientation B (Fig. 2B)].

As mentioned above, the bright regions are actually slightly longer than a phenylbenzoate unit should be. Because simple alkyl units should be dark, it is attractive to assume that the extra length in the bright regions is related somehow to the epoxide unit. Furthermore, in the best images not only is the pairing chiral in two dimensions, but what appear to be the individual molecular components of the crystal are chiral in two dimensions as well, with the chirality manifested by bright regions off the row axis and overlapping between rows. This suggested to us that the epoxide units are at the overlapping side of the phenylbenzoates, as indicated in orientation A. Thus, the basic structural motif of Fig. 2A was explored with molecular mechanics.

First, a gas phase conformational search of the MDW 74 structure was done with the Dreiding II force field in the POLYGRAF (Molecular Simulations, Burlington, Massachusetts) molecular modeling program (*12*). A total of 27,930 conformations were screened by energy, and all minima were further screened according to how well each one "fit" on a graphite surface. A "best fit" conformation was chosen, this conformation being only slightly above the lowest energy conformation found.

A 2D crystal of MDW 74 was constructed according to the assumptions outlined previously. A pair of molecules was placed on the center of a modeled graphite sheet in orientation A, surrounded by 16 more molecules, and this unit was surrounded by 14 more molecules. The inner 18 molecules were allowed to move freely during the computations, while the graphite and the outer 14 molecules were fixed. After an initial short minimization, the ensemble was run through 10 to 20 cycles, each consisting of 50 steps of molecular dynamics (*13*) followed by 50 steps of minimization. The central pair of molecules was then analyzed, and the lower energy conformation was used to construct a new 2D crystal. This process was repeated until the total energy of the crystal no longer decreased after a run.

The central conformation found in this way was then compared to the global minimum found in the gas phase conformational search. Although the conformation from the crystal was initially several kilocalories per mole higher in energy than the gas phase minimum, a gas phase minimization of the crystal conformation afforded a very similar conformation that was several kilocalories per mole in energy below the previously found "global minimum." Thus, the computed conformation in the 2D crystal model is readily accessible from the best computed gas phase minimum found to date.

A major difficulty with all STM studies of

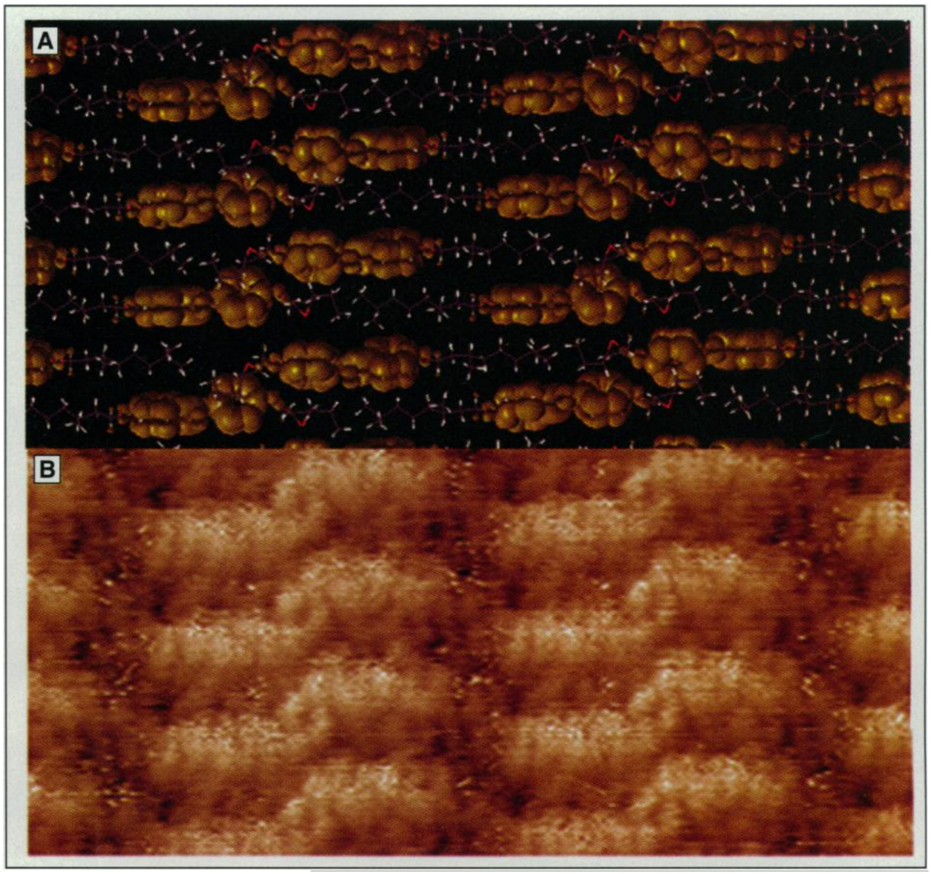

Fig. 4. Molecular mechanics modeling and molecular orbitals in superposition, along with an STM image of MDW 74. (**A**) Molecular model of MDW 74 on graphite, with lowest four unoccupied orbitals; (**B**) STM image of MDW 74 on graphite (raw data).

adsorbed molecules is interpreting the images. How an adsorbed molecule influences tunneling efficiency, and particularly how different parts of a molecule may influence the tunneling efficiency differently, giving rise to the observed contrast in STM images, is poorly understood at best. Many mechanisms have been proposed to explain this contrast (*14*). One proposal is that the contrast is a result of interactions between the tunneling electrons and the molecular orbitals of the adsorbate. Several studies have shown a correlation between STM images and the single highest occupied molecular orbital (HOMO) or the lowest unoccupied molecular orbital (LUMO) of the adsorbed molecule (*15*). In several cases the HOMO and LUMO were sufficiently similar that it could not be determined if one, the other, or both were contributing to contrast in the STM image. Although adsorption may alter molecular orbital energies from their gas phase values, studies have suggested that this change is small (*16*).

To pursue this line of analysis, frontier molecular orbitals of MDW 74 were calculated by the Spartan (Wavefunction, Irvine, California) molecular modeling program. Calculations were performed at both semiempirical [modified neglect of differential overlap (MNDO)] and ab initio [Hartree–Fock/STO-3G (HF/STO-3G)] levels; except for absolute energies, the results were very similar. The orbitals calculated with MNDO (Fig. 3) showed that neither the single HOMO nor the single LUMO alone could explain the observed contrast because the HOMO and LUMO are each localized on one ring of the phenylbenzoate system, even though both rings appeared bright in the STM images. However, the observed contrast could be explained equally well by the group of four highest occupied orbitals (Fig. 3E), the group of four lowest unoccupied orbitals (Fig. 3C), or a combination of both (Fig. 3D).

The modeling work is summarized in Fig. 4, which shows a framework model of the 2D crystal computed by molecular mechanics with superimposed orbitals (LUMOs shown in Fig. 3C), along with the STM image itself. The one feature of the STM image that the model does not reproduce is the dissymmetry in the center of each column. Although it seems likely that this feature is associated with the epoxide group, their exact relationship is unclear. For a better test of the connection between molecular orbitals and STM images, high-resolution STM images of molecules possessing additional functional groups must be obtained.

REFERENCES AND NOTES

1. D. P. E. Smith, H. Hörber, Ch. Gerber, G. Binnig, *Science* **245**, 43 (1989).
2. For a recent review, see J. Frommer, *Angew. Chem. Int. Ed. Engl.* **31**, 1298 (1992).
3. Selected references: M. Shigeno *et al.*, *Jpn. J. Appl. Phys.* **29**, L119 (1990); D. P. E. Smith, *J. Vac. Sci. Technol. B* **9**, 1119 (1991); Y. Iwakabe *et al.*, *Jpn. J. Appl. Phys.* **30**, 2542 (1991).
4. J. K. Spong, L. J. LaComb Jr., M. M. Dovek, J. E. Frommer, J. S. Foster, *J. Phys. France* **50**, 2139 (1989); J. K. Spong *et al.*, *Nature* **338**, 137 (1989); J. S. Foster, J. E. Frommer, J. K. Spong, *SPIE* **1080**, 200 (1989); H. Shindo *et al.*, *Chem. Commun.* **1990**, 760 (1990); M. Hara, T. Umemoto, H. Takezoe, A. F. Garito, H. Sasabe, *Jpn. J. Appl. Phys.* **30**, L2052 (1991); S. L. Brandow *et al.*, *Liq. Cryst.* **13**, 163 (1993).
5. D. C. Parks, N. A. Clark, D. M. Walba, P. D. Beale, *Phys. Rev. Lett.* **70**, 607 (1993).
6. For the images in Fig. 1, the MDW 74 sample was >99% stereochemically pure at the epoxide stereocenters and about 80% stereochemically pure at the tertiary alkyl stereocenter (that is, the material was an 80:20 mixture of diastereomers differing at the tertiary alkyl stereocenter). Many other similar (though lower resolution) images were obtained with MDW 74 of >98% diastereomeric purity.
7. The current working hypothesis is that a very rare tip configuration produced the best STM images.
8. Only phenylbenzoates unsubstituted ortho to the ester moiety were chosen. The search found 57 fragments in 36 molecules. The minimum dihedral angle found was 42°; the average dihedral was 88°.
9. A. J. Groszek, *Proc. R. Soc. London Ser. A.* **314**, 473 (1970); U. Bien-Vogelsang and G. H. Findenegg, *Colloids Surf.* **21**, 469 (1986); G. H. Findenegg and M. Liphard, *Carbon* **25**, 119 (1987).
10. W. Mizutani, M. Shigeno, M. Ono, K. Kajimura, *Appl. Phys. Lett.* **56**, 1974 (1990).
11. D. P. E. Smith, W. M. Heckl, H. A. Klagges, *Surf. Sci.* **278**, 166 (1992); K. Matsushige *et al.*, *Jpn. J. Appl. Phys.* **32**, 1716 (1993).
12. Now Cerius^2.
13. Adiabatic dynamics, 300 K, 0.001-ps time step.
14. J.-Y. Yuan and Z. Shao, *Ultramicroscopy* **34**, 223 (1990); W. Mizutani, M. Shigeno, K. Kajimura, M. Ono, *ibid.* **42–44**, 236 (1992); M. M. D. Ramos, *J. Phys.: Condens. Matter* **5**, 2843 (1993); H. Ou-Yang, R. A. Marcus, B. Källebring, *J. Chem. Phys.* **100**, 7814 (1994).
15. P. H. Lippel, R. J. Wilson, M. D. Miller, Ch. Wöll, S. Chiang, *Phys. Rev. Lett.* **62**, 171 (1989); H. Nejoh, *Appl. Phys. Lett.* **57**, 2907 (1990); D. P. E. Smith, J. K. H. Hörber, G. Binnig, H. Nejoh, *Nature* **344**, 641 (1990); M. Shigeno, M. Ohmi, M. Suginoya, W. Mizutani, *Mol. Cryst. Liq. Cryst.* **199**, 141 (1991); S. Richter and Y. Manassen, *J. Phys. Chem.* **98**, 2941 (1994); C. Ludwig, B. Gompf, J. Petersen, R. Strohmaier, W. Eisenmenger *Z. Phys. B* **93**, 365 (1994).
16. A. J. Fisher, P. E. Blöchl, *Phys. Rev. Lett.* **70**, 3263 (1993); K.-H. Frank, R. Dudde, E. E. Koch, *Chem. Phys. Lett.* **132**, 83 (1986).
17. This work was supported in part by the Office of Naval Research and by the National Science Foundation (grants DMR-9202312 and DMR-9224168).

30 August 1994; accepted 6 December 1994

Optical Properties of the South Pole Ice at Depths Between 0.8 and 1 Kilometer

P. Askebjer, S. W. Barwick, L. Bergström, A. Bouchta, S. Carius,
A. Coulthard, K. Engel, B. Erlandsson, A. Goobar,[*] L. Gray,
A. Hallgren, F. Halzen, P. O. Hulth, J. Jacobsen, S. Johansson,[†]
V. Kandhadai, I. Liubarsky, D. Lowder, T. Miller,[‡] P. C. Mock,
R. Morse, R. Porrata, P. B. Price, A. Richards, H. Rubinstein,
E. Schneider, Q. Sun, S. Tilav, C. Walck, G. Yodh

The optical properties of the ice at the geographical South Pole have been investigated at depths between 0.8 and 1 kilometer. The absorption and scattering lengths of visible light (~515 nanometers) have been measured in situ with the use of the laser calibration setup of the Antarctic Muon and Neutrino Detector Array (AMANDA) neutrino detector. The ice is intrinsically extremely transparent. The measured absorption length is 59 ± 3 meters, comparable with the quality of the ultrapure water used in the Irvine-Michigan-Brookhaven and Kamiokande proton-decay and neutrino experiments and more than twice as long as the best value reported for laboratory ice. Because of a residual density of air bubbles at these depths, the trajectories of photons in the medium are randomized. If the bubbles are assumed to be smooth and spherical, the average distance between collisions at a depth of 1 kilometer is about 25 centimeters. The measured inverse scattering length on bubbles decreases linearly with increasing depth in the volume of ice investigated.

The AMANDA project was conceived to exploit polar ice as a transparent and sterile detection medium with a large volume for the detection of muons and neutrinos from astrophysical sources. Photomultiplier tubes (PMTs) deployed in the South Pole ice sense the Cherenkov light emitted by highly relativistic muons. Down-going muons originate from cosmic-ray showers, and nearly isotropic muons result from interactions between neutrinos and nucleons in the ice around and the bedrock below the detector. Polar ice, unlike ocean water which has also been proposed as a neutrino detector medium [for example, in the DUMAND (Deep Underwater Muon and Neutrino Detector) and NESTOR (neutrinos from supernovae and TeV sources, ocean range) experiments (*1*, *2*)], is free of bioluminescent organisms and natural radioactive isotopes such as $^{40}\mathrm{K}$. In addition, the ice forms a rigid support structure for